Structural Dynamics of the α-Neurotoxin−Acetylcholine-Binding Protein Complex: Hydrodynamic and Fluorescence Anisotropy Decay Analyses†

Ryan E. Hibbs,‡,§ David A. Johnson,‖ Jianxin Shi,‡ Scott B. Hansen,‡ and Palmer Taylor*,‡

Department of Pharmacology and Biomedical Sciences Graduate Program, University of California−San Diego, La Jolla, California 92093-0636, and Division of Biomedical Sciences, University of California−Riverside, Riverside, California 92521-0121

Received August 28, 2005; Revised Manuscript Received October 24, 2005

ABSTRACT: The three-fingered α-neurotoxins have played a pivotal role in elucidating the structure and function of the muscle-type and neuronal α7 nicotinic acetylcholine receptors (nAChRs). To advance our understanding of the α-neurotoxin−nAChR interaction, we examined the flexibility of α-neurotoxin bound to the acetylcholine-binding protein (AChBP), which shares structural similarity and sequence identities with the extracellular domain of nAChRs. Because the crystal structure of five α-cobratoxin molecules bound to AChBP shows the toxins projecting radially like propeller "blades" from the perimeter of the donut-shaped AChBP, the toxin molecules should increase the frictional resistance and thereby alter the hydrodynamic properties of the complex. α-Bungarotoxin binding had little effect on the frictional coefficients of AChBP measured by analytical ultracentrifugation, suggesting that the bound toxins are flexible. To support this conclusion, we measured the anisotropy decay of four site-specifically labeled α-cobratoxins (conjugated at positions Lys^{23}, Lys^{35}, Lys^{49}, and Lys^{69}) bound to AChBP and free in solution and compared their anisotropy decay properties with fluorescently labeled cysteine mutants of AChBP. The results indicated that the core of the toxin molecule is relatively flexible when bound to AChBP. When hydrodynamic and anisotropy decay analyses are taken together, they establish that only one face of the second loop of the α-neurotoxin is immobilized significantly by its binding. The results indicate that bound α-neurotoxin is not rigidly oriented on the surface of AChBP but rather exhibits segmental motion by virtue of flexibility in its fingerlike structure.

Nicotinic acetylcholine receptors (nAChRs)[1] are prototypic members of the Cys-loop superfamily of pentameric ligand-gated ion channels, so named by a conserved disulfide linkage in the extracellular domain of the receptors (*1*). Other members of this family include the $GABA_A$, $GABA_C$, $5\text{-}HT_3$, and glycine receptors. nAChRs are responsible for fast neurotransmission via acetylcholine-induced cation permeability at the skeletal neuromuscular junction, as well as at ganglionic and central nervous system synapses. Various subtypes of nAChRs are defined by the subunit composition of the homo- or heteropentameric subunit assemblies; ligand specificity is governed by binding determinants at the subunit interface.

Our understanding of the structure and function of nAChRs in particular and ligand-gated ion channels in general has been greatly facilitated by studies of the muscle-type nAChR and snake venom α-neurotoxins from *Elapidae* species, which display high specificity for muscle-type nAChRs (*2*). α-Bungarotoxin, a member of this family of over 100 α-neurotoxins, enabled the first isolation and characterization of a nAChR (*3*). Other *Elapidae* α-neurotoxins have also been of great value in the identification and *in situ* localization of nAChRs (*4*). Structurally, α-neurotoxins consist of a core region from which three loops extend outward like fingers from a hand. The secondary structure consists of two antiparallel *β*-sheets, one of which is a three-stranded *β*-sheet with two strands associated with the central finger (loop II). Functionally, the α-neurotoxins are defined by their ability to compete with acetylcholine at postsynaptic nicotinic receptors and were hence originally denoted "curaremimetic toxins". α-Bungarotoxin and α-cobratoxin fall into the category of long-chain (type II) α-neurotoxins, which contain four internal core disulfides and one residing at the tip of their central loop (loop II). These long-chain family members share a high affinity for the skeletal muscle type and the homomeric α7 neuronal nAChR.

Recently, the crystal structure for the acetylcholine-binding protein (AChBP), a valuable structural (*1*, *5*) and functional (*6*) surrogate of the nicotinic receptor ligand-binding domain, complexed with α-cobratoxin, was solved at 4.2 Å resolution (*7*). This structure complemented longstanding biochemical,

† Supported by R37-GM18360 to P.T., IBN-9515330 to D.A.J., and a Pharmaceutical Research Manufacturers of America Foundation predoctoral fellowship to R.E.H.

* To whom correspondence should be addressed: Department of Pharmacology, University of California−San Diego, 9500 Gilman Drive, La Jolla, CA 92093-0636. E-mail: pwtaylor@ucsd.edu. Telephone: 858-534-1366. Fax: 858-534-8248.

‡ Department of Pharmacology, University of California−San Diego.

§ Biomedical Sciences Graduate Program, University of California−San Diego.

‖ University of California−Riverside.

[1] Abbreviations: AChBP, acetylcholine-binding protein; nAChR, nicotinic acetylcholine receptor; FITC, fluorescein isothiocyanate; MTS-EDANS, *N*-(methanethiosulfonylethylcarboxamidoethyl)-5-naphthylamine-1-sulfonic acid; MTS-Fl, 2-[(5-fluoresceinyl)aminocarbonyl]ethyl methanethiosulfonate; SDS−PAGE, sodium dodecyl sulfate−polyacrylamide gel electrophoresis; GnTI⁻, *N*-acetylglucosaminyltransferase I deficient cell line.

10.1021/bi051735p CCC: $30.25
Published on Web 11/24/2005

mutagenesis, and structure-based modeling studies on α-neurotoxin binding to nAChRs (*8*−*12*) and suggested new, unpredicted atomic interactions of the toxin with the receptor.

To advance our understanding of the interaction of α-neurotoxins with nicotinic receptors, we examined the conformational flexibility of α-neurotoxins bound to AChBP, focusing on the orthologous peptides α-cobratoxin and α-bungarotoxin. Because the crystal structure of five α-cobratoxin molecules bound to AChBP shows the toxins projecting radially, like propeller "blades", from the outer perimeter of the cylindrical AChBP, we reasoned that, if the "blades" were rigid, they should dramatically increase the hydrodynamic, frictional drag or resistance of the α-neurotoxin−AChBP complex. Hydrodynamic properties of detergent-solubilized receptors from *Torpedo* have been studied (*13*); however, by examining only the extracellular domain of this protein family, the subunit size falls in a range where bound α-neurotoxin molecules should influence hydrodynamic characteristics.

The diffusion and frictional coefficients of the α-neurotoxin-bound and unliganded AChBP were measured using analytical ultracentrifugation. We found that α-neurotoxin binding had little effect on the frictional coefficients, revealing a minimal apparent difference in dimensional asymmetry between AChBP and its toxin complex. This suggested a significant level of flexibility of the bound α-neurotoxin in the time domain of translational diffusion of AChBP. To confirm independently the flexibility of the bound α-neurotoxins, we measured the anisotropy decay of four site-specifically FITC (fluorescein isothiocyanate)-labeled α-cobratoxins bound to AChBP and free in solution and compared their decays to those of fluorescently labeled cysteine mutants of AChBP. The results indicate that the internal core and most finger residue positions of the toxin molecule are relatively flexible when bound to AChBP.

MATERIALS AND METHODS

Ligands and Labeling Reagents. α-Bungarotoxin was purchased from Sigma−Aldrich (St. Louis, MO). [^{125}I]-α-Bungarotoxin (specific activity: 130 Ci/mmol) was a product of Perkin−Elmer Life Sciences, Inc. (Wellesley, MA). α-Cobratoxin was isolated as previously described from the venom of *Naja naja siamensis* (Miami Serpentarium, Salt Lake City, UT) (*14*). 2-[(5-Fluoresceinyl)aminocarbonyl]-ethyl methanethiosulfonate (MTS-Fl) and *N*-(methanethiosulfonylethylcarboxamidoethyl)-5-naphthylamine-1-sulfonic acid (MTS-EDANS, Figure 1) were purchased from Toronto Research Chemicals, Inc. (Ontario, Canada). All other chemicals were of the highest grade commercially available.

Expression, Mutagenesis, and Purification of AChBP. Wild-type AChBP from *Lymnaea stagnalis* was expressed from a cDNA synthesized from oligonucleotides selected for mammalian codon usage, as previously described (*15*). Briefly, the cDNA was inserted into a p3×FLAG-CMV-9 expression vector (Sigma) containing a preprotrypsin leader peptide followed by an NH_2-terminal 3×FLAG epitope. A COOH-terminal 6×-histidine tag was attached for radioligand-binding assays. Stable cell lines of single cysteine mutants of AChBP were generated as previously described (*16*). For protein used in the hydrodynamic assays, wt-AChBP cDNA was also transfected and stably selected in an HEK 293 cell line deficient in the *N*-acetylglucosaminyltransferase I gene ("GnTI$^-$ cells"), which should result in homogeneous glycosylation of limited oligosaccharide length (*17*, *18*). The expression vector for AChBP differed slightly in the GnTI$^-$ cell line in that the construct contained a 1×NH_2-terminal FLAG epitope and no COOH-terminal tag. AChBP was purified from the tissue culture medium by adsorption onto an α-FLAG antibody column and elution with the FLAG peptide as previously described (*16*). Purity and assembly of subunits as a pentamer were assessed by SDS−PAGE and fast protein liquid chromatography.

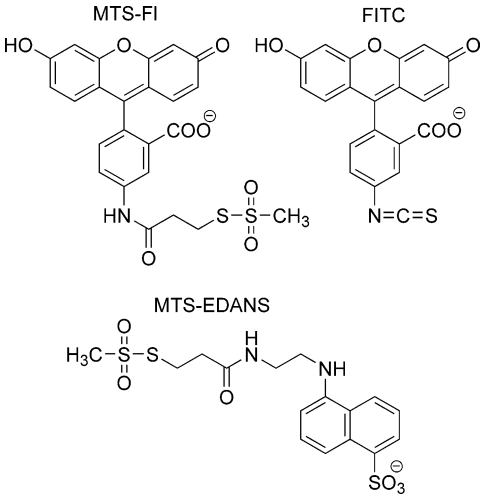

FIGURE 1: Chemical structures of fluorescent probes used in protein labeling. FITC was conjugated to lysine residues in α-cobratoxin, MTS-fluorescein, and MTS-EDANS to cysteine residues in AChBP for anisotropy decay analysis.

Fluorophore Labeling. Four site-specifically FITC-conjugated α-cobratoxins, labeled at positions of Lys^{23}, Lys^{35}, Lys^{49}, and Lys^{69}, were prepared as previously described (*19*). MTS-Fl and MTS-EDANS labeling of two cysteine-substituted AChBPs at positions N158C and D194C was carried out in a 100 μL volume containing 20 μM AChBP (subunit or binding site concentration) and 100 μM fluorophore in 50 mM Tris-HCl, 150 mM NaCl, and 0.02% NaN_3 at pH 7.4. Labeling reactions ran for 90 min at room-temperature shielded from light, after which free fluorophore was removed by buffer exchange (4× 2 mL washes) into 0.1 M $NaPO_4$ at pH 7.0 in Centricon YM-30 spin columns (Millipore, Billerica, MA). Specific labeling was assessed by a comparison of fluorophore emission from the labeled mutant with that of a sample of wt-AChBP that was labeled in parallel with the mutant, after standardization to the protein concentration by the Bradford assay. In all cases, nonspecific labeling was ≤5%. Stoichiometry of labeling for each preparation was estimated from a comparison of the fluorophore concentration (absorbance at 340 nm for MTS-EDANS; extinction coefficient, ~5700 M^{-1} cm^{-1}, and at 496 nm for MTS-4-fluorescein; extinction coefficient, 85 000 M^{-1} cm^{-1}) and the protein concentration (by absorbance at 280 nm; extinction coefficient, 268 000 M^{-1} cm^{-1}). Stoichiometry of subunit labeling in each mutant preparation ranged between 20 and 25%.

Mass Spectrometry. Matrix-assisted laser desorption/ionization−time-of-flight mass spectrometry was performed on a PE Biosystems Voyager DE-STR instrument (Framing-

ham, MA). Purified recombinant AChBPs at 2 mg/mL in 60% acetonitrile and 0.1% (v/v) trifluoroacetic acid were mixed 1:1 with a matrix of 10 mg/mL saturated sinapinic acid (3,5-dimethoxy-4-hydroxycinnamic acid) dissolved in 50% acetonitrile and 0.1% trifluoroacetic acid at pH 2.2. Droplets (1 μL) of the AChBP/matrix mixture, containing approximately 6 pmol of protein, were spotted and dried by slow evaporation. Mass spectra were collected using the linear mode, and external calibration was performed using yeast enolase protein (+1 and +2 monomer *m*/*z* species) and horse skeletal apomyoglobin (+1 monomer *m*/*z*).

Analytical Ultracentrifugation. Sedimentation equilibrium and velocity experiments were conducted at 20 °C using a Beckman Optima XL-1 analytical ultracentrifuge equipped with absorbance optics at 280 nm and an An60Ti rotor. Sedimentation equilibrium experiments were performed with protein solutions of 200 μg/mL centrifuged at 8, 10, and 12 krpm, in charcoal-filled Epon 6 channel centerpieces loaded with 110 μL of sample and 125 μL of reference buffer (50 mM Tris-HCl, 150 mM NaCl, and 0.02% NaN_3 at pH 7.4). Individual samples were centrifuged for 16 h at each speed with an absorbance scan conducted every 2 h. Data were collected in step mode with a spacing of 0.001 cm. Values presented are an average of at least three absorbance scans at each speed. Equilibrium was achieved as judged by a comparison of overlays of three subsequent absorbance scans. The partial specific volume of the AChBPs was calculated using the Sednterp computer program (version 1.07, Hayes, Laue, Philo, University of New Hampshire, 2002) to be 0.71 with no ligand present and with α-bungarotoxin bound. The ligand was added to achieve a slight excess of binding stoichiometry (1.2 molecules of ligand/binding site). Stoichiometry of α-neurotoxin binding to AChBP was demonstrated previously using SDS−PAGE (*7*).

Sedimentation velocity experiments were performed at 30 000 rpm in charcoal-filled Epon double-sector centerpieces loaded with 400 μL of sample (200 μg/mL) and 425 μL of reference buffer (as above). Migration rates were monitored in a continuous scan mode and were analyzed using the DCDT+ computer program (version 1.16, Philo). The reported weight-averaged sedimentation coefficients ($S_{20,w}$) obtained from DCDT+ are calculated by a weighted integration over the entire range of sedimentation coefficients covered by the $g(s)$ distribution (*20*) and corrected for the solution density and viscosity (*21*). Sedimentation data were collected on samples at two concentrations (0.2 A units and 0.4 A units), and a concentration dependence of *s* was not observed (data not shown).

From an experimentally determined sedimentation coefficient (s), the apparent frictional coefficient f can be calculated with the expression

$$f = \frac{M(1 - \bar{V}\rho)}{N_A s} \quad (1)$$

and a frictional coefficient ratio f/f_0 equal to the Perrin shape factor (F), where f_0 is a theoretical minimum frictional coefficient for a nonhydrated sphere of a given molecular weight

$$f_0 = 6\pi\eta r_0 \quad (2)$$

where

$$r_0 = (3M\bar{V}/4\pi N_A)^{1/3} \quad (3)$$

and M is the molecular weight of the protein, $\bar{V}$ is the partial specific volume of the protein, ρ is the density of protein in g/cm^3, N_A equals 6.02×10^{23}, and η is the solution viscosity. For our analysis, M was determined by mass spectrometry and $\bar{V}$, ρ, and η were calculated on the basis of the amino acid content with the Sednterp computer program. From f, a diffusion constant D can be calculated with the expression

$$D = \frac{kT}{f} \quad (4)$$

where k equals 1.38×10^{-16} erg × deg^{-1} and T is the absolute temperature (*22*).

Radioligand-Binding Assays. A scintillation proximity assay (SPA, Amersham Biosciences) was adapted for use in a soluble radioligand-binding assay (*16*). Briefly, AChBP (0.5 nM binding sites) was incubated with 20 nM [^{125}I]-labeled α-bungarotoxin in a solution of 0.1 mg/mL anti-His SPA beads, and FITC-labeled α-cobratoxin was added in increasing concentrations. Binding data were fit to a one-site competition model using the Prism 4 computer program (GraphPad Software, Inc.). All radioligand binding data are averages of at least three replicate experiments.

Time-Resolved Fluorescence Anisotropy. Emission anisotropy was determined by time-correlated single-photon counting with an HORIBA Jobin Yvon IBH Ltd. (Glasgow, U.K.) 470-nm NanoLED laser (with FITC of MTS-Fl conjugates) or a 375-nm NanoLED laser (with the MTS-EDANS conjugate) run at 1 MHz, an HORIBA Jobin Yvon IBH Ltd. model TBX-04 photon detector, a rotatable Glan−Thomson polarizer placed in the path of the excitation beam, and a rotatable Polaroid HNP′B dichroic film polarizer placed in front of the photon detector. A depolarizing filter was also placed between the emission polarizer and photon detector to minimize the polarization bias of the photon detector. Vertically, $I_{\parallel}(t)$, and orthogonally, $I_{\perp}(t)$, polarized emission components were collected at 22 °C, while the samples were excited with vertically polarized light. For FITC and MTS-Fl, excitation and emission bands were selected with Omega 470DF35 and Omega 510DF23 filters, respectively. For MTS-EDANS, excitation and emission bands were selected with Corning 4-70 interference and Oriel 470 nm cuton filters, respectively. Typically, $4-6 \times 10^4$ peak counts were collected (in 2 min) with the emission polarizer oriented vertically. The orthogonal emission decay profile was generated over the same time interval. To minimize convolution artifacts, laser profiles were recorded by removing the emission filter and monitoring light scatter from a suspension of latex beads. The data analysis software corrected for the wavelength-dependent temporal dispersion of the photoelectrons by the photon detector. The polarization bias (G) of the detection instrumentation was determined by measuring the integrated photon counts/6×10^6 lamp flashes, while the samples were excited with orthogonally polarized light and the emission was monitored with a polarizer oriented in the vertical and orthogonal directions (G equals 1.015).

Unless stated otherwise, emission anisotropy decay was analyzed with the impulse reconvolution method implemented in the DAS6 software package from HORIBA Jobin Yvon IBH Ltd. (Glasgow, U.K.) described elsewhere (*23*).

Briefly and simply, this approach splits the analysis into two steps: analysis of the total emission decay, $S(t)$, followed by analysis of the vertical/perpendicular difference emission decay, $D(t)$. $S(t)$, free of anisotropy effects, is given by the expression

$$S(t) = I_{||}(t) + GI_{\perp}(t) \quad (5)$$

and was analyzed as a bi-exponential function. $D(t)$, which includes both fluorescence and anisotropy parameters, is given by the expression

$$D(t) = I_{||}(t) - GI_{\perp}(t) \quad (6)$$

$D(t)$ is deconvolved with the results from the $S(t)$ analysis as a constraint yielding

$$r(t) = \beta_1 \exp(-t/\phi_{fast}) + \beta_2 \exp(-t/\phi_{slow}) \quad (7)$$

Here, β_1 and β_2 are the amplitudes of the anisotropy at time 0 for the fast and slow anisotropy decay processes, respectively. ϕ_{fast} and ϕ_{slow} are the fast and slow rotational correlation times of the anisotropy decay, respectively. A nonassociative model was assumed, where the emission relaxation times are common to all of the rotational correlation times. Goodness of fit was evaluated from the values of the reduced χ^2_r and by visual inspection of the weighted-residual plots.

RESULTS

Hydrodynamic Analyses of AChBP and the α-Neurotoxin Complex. In sedimentation equilibrium (Figure 2A), sample solutions are centrifuged until equilibrium is approached where the concentration from the centrifugal force is balanced by diffusion from a concentration gradient extending in the opposite direction. Because dimensional asymmetry of the macromolecule affects both of these forces equally, sedimentation equilibrium measurements provide an estimate of molecular weight independent of the volume and shape of the hydrated macromolecule. Mass spectrometry was used as an independent assessment of molecular weight to verify the hydrodynamic results. In all cases, measurements from the two methods yielded data within 5% (Table 1).

To serve as an internal control, AChBP produced in a HEK 293 cell line deficient in the glycosylation-processing enzyme, *N*-acetylglucosaminyltransferase I (GnTI$^-$), was also examined by mass spectrometry and analytical ultracentrifugation. The corresponding molecular-weight difference between this protein species and that produced in standard HEK 293 cells can be attributed to the mass difference in the conjugated affinity tags and the oligosaccharide trimming to 5 mannose residues and 2 *N*-acetylglucosamine residues per AChBP subunit derived from GnTI$^-$ HEK cells (*18*). The respective mass differences are 3×FLAG plus 6×His in the standard protein species, versus 1×FLAG, 12 800 Da, and the absence of oligosaccharide processing, 6800 Da in the glycosylation-processing-deficient species. Differences in molecular weight and the mass uniformity of the trimmed oligosaccharide structure are qualitatively evident upon SDS gel electrophoresis (Figure 2B).

Sedimentation velocity measurements were used to measure the effect of ligand binding on the overall volume and shape of AChBP. Here, differences in dimensional asymmetry are monitored for molecules of established molecular weight, and the protein concentration change over the length of the sample cell in relation to time (Figure 3) is used to determine sedimentation, translational diffusion, and frictional coefficients.

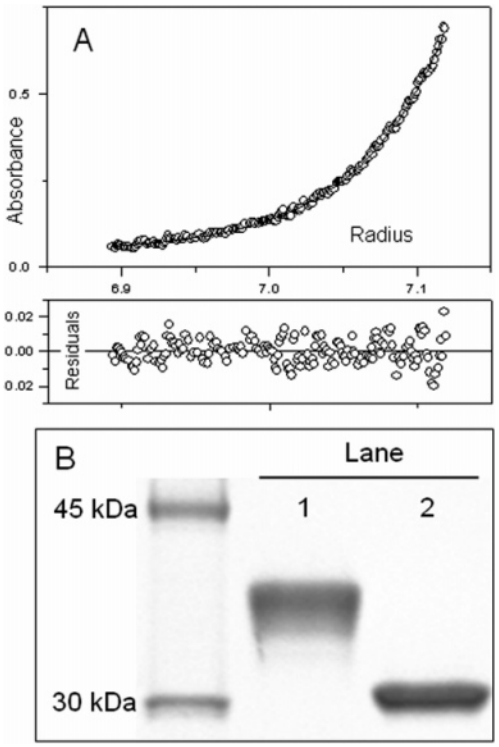

FIGURE 2: Characterization of AChBP by sedimentation and gel electrophoresis. (A) Sedimentation equilibrium of AChBP from HEK 293 cells with α-bungarotoxin present. Samples of 110 μg/mL AChBP and a 1.2 molar excess of α-bungarotoxin (in 50 mM Tris-HCl and 150 mM NaCl at pH 7.4) were centrifuged at 10 000 rpm until a constant profile was established as determined by an overlay of consecutive absorbance scans. These data were fit to an equation corresponding to a molecular weight of 188 000 Da for the complex. (B) SDS−PAGE of the purified AChBPs from HEK 293 cells (lane 1) and GnTI$^-$ cells (lane 2). A total of 1 μg of protein was run in each lane of a 16% polyacrylamide gel.

We also used sedimentation velocity to monitor the effect of α-bungarotoxin (Figure 4) binding on the macromolecular translational diffusion parameters of AChBP. Binding of five 8-kD toxin molecules to AChBP slightly increased the sedimentation coefficient from 6.9 to 8.1 S (Table 1). A similar small increase from bound α-neurotoxin was observed in the sedimentation coefficient for the differentially glycosylated AChBPs. The diffusion coefficients associated with AChBP from GnTI$^-$ cells were slightly higher than for the heavily glycosylated form, consistent with a trimming of an extended and presumably more heterogeneous oligosaccharide as well as the histidine tag. Notably, there was no significant change in the frictional coefficient ratio f/f_0 upon α-neurotoxin binding to either species of AChBP. As an internal control, parallel hydrodynamic experiments were performed using α-cobratoxin, and indistinguishable sedimentation parameters were obtained (data not shown). Binding of the high-affinity agonist epibatidine (MW of 209 D) had no detectable effect on the sedimentation parameters.

Fluorescence Anisotropy. To examine more directly the flexibility of the bound α-neurotoxin, time-resolved anisotropy decay of reporter groups specifically conjugated to sites

Table 1: Experimentally Determined Sedimentation Parameters[a]

	MW by mass spectrometry[b]	MW by sedimentation equilibrium	S ($\times 10^{-13}$ s)	D (cm^2/s)	f/f_0
apo	151 945	151 000	6.9	3.9	1.5
+ epibatidine	152 990	152 000	6.8	3.8	1.6
+ α-bungarotoxin	191 868	188 000	8.1	3.6	1.5
apo GnTI$^-$	130 305	127 000	6.8	4.5	1.4
+ α-bungarotoxin GnTI$^-$	170 229	164 000	8.3	4.3	1.3

[a] Molecular weights were determined by mass spectrometry and sedimentation equilibrium. Sedimentation coefficients in Svedbergs (S), diffusion constants in cm^2/s, and frictional coefficients were determined by sedimentation velocity, using the MW determined by mass spectrometry. [b] Increase in MW upon ligand binding is the calculated sum of the apo-receptor-measured value plus the projected addition of five ligand molecules.

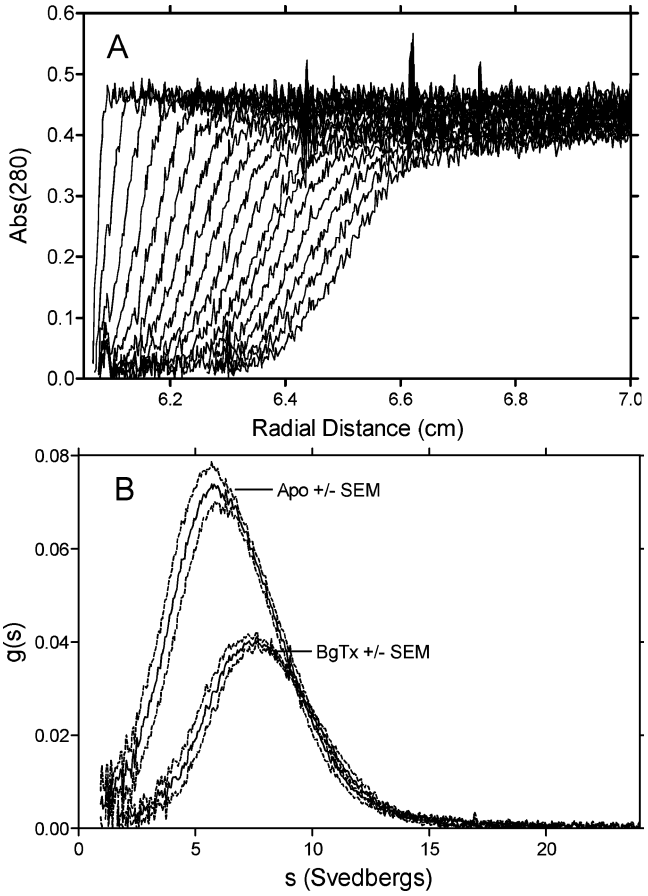

FIGURE 3: Sedimentation velocity of AChBP from HEK 293 cells. (A) Raw data taken as radial absorbance scans at 10 min intervals with apo protein (no ligand present). (B) Analyzed values ± SEM presented as $g(s)$ versus s, comparing apo protein to that with α-bungarotoxin added. The difference in the curve amplitude here is due to a 2-fold higher concentration used for apo-protein data. Weight-averaged sedimentation coefficients (s) were calculated using the fitting equation described in the Materials and Methods to be 6.9 and 8.1 S for apo and the α-bungarotoxin complex, respectively.

on α-cobratoxin and sites of cysteine substitution on AChBP were measured free in solution and in a complexed state. We have previously reported that it is often possible to resolve to a significant degree tether arm torsional motions of the reporter groups about their linkages to the α-carbon backbone (<1 ns; very fast), local segmental mobility of the α-carbon backbone (low nanoseconds; fast), and global rotation of the macromolecule (slow) (*24*−*27*). Here, FITC was separately conjugated to the ϵ-amino groups of four lysines in α-cobratoxin (FITC-Lys^{23}, FITC-Lys^{35}, FITC-Lys^{49}, and FITC-Lys^{69}, Figure 4A). Lys^{23} is located in loop II in the center of three antiparallel β-strands; Lys^{35} is in a less structured region near the tip of loop II; Lys^{49} is positioned on loop III; and Lys^{69} is near the C terminus of the toxin. For a comparison, MTS-Fl was conjugated to the sulfhydryl side chains of substituted cysteines on two AChBP mutants (N158C and D194C). Additionally, MTS-EDANS, a long lifetime reporter group, was conjugated to the substituted cysteine in the D194C AChBP mutant to better assess the averaged whole-body rotational correlation time of the α-neurotoxin−AChBP complex. Radioligand-binding assays on the fluorescent α-cobratoxin derivatives were performed with AChBP and showed that covalent modification did not alter the binding parameters by more than 5-fold (Table 2).

The anisotropy decay profiles of the FITC-α-cobratoxins free in solution were well-fit to a bi-exponential expression (eq 7), with the slow rotational correlation times (ϕ_{slow}) ranging between 3.5 and 4.5 ns (Figure 5 and Table 3). These values are close to the value predicted by the Stokes−Einstein equation (3.2 ns) for an 8-kD spherical protein, strongly suggesting that the ϕ_{slow} values reflect the average rotational correlation time of the toxin with its modest dimensional asymmetry (*28*). With the exception of the FITC-Lys^{23} derivative, the ϕ_{fast} values were <1 ns, indicating a high level of mobility of the reporter groups (at Lys^{35}, Lys^{49}, and Lys^{69}) and that rates of the tether arm and local α-carbon backbone motions around sites of conjugation overlap one another and are irresolvable (*29*). The ϕ_{fast} value of the FITC conjugated to Lys^{23}, however, was significantly greater than 1 ns (1.8 ns). With the ϕ_{slow} value of the FITC-Lys^{23} derivative reflecting the whole-body rotational correlation time, the ϕ_{fast} value for this conjugate largely reflects local backbone diffusional processes around Lys^{23}. All of this indicates that the backbone motions around Lys^{23} are significantly less than that of the other sites of conjugation examined, which is not surprising given the position of the Lys^{23} residue centrally located within three antiparallel β-strands and the low thermal (B) factor values of both the main- and side-chain atoms of this residue compared to the other lysines (Figure 4A, PDB accession code 2CTX). Because of the short global rotational correlation times, we were not able to resolve differences in the backbone mobility of the other labeling positions; however, our results with position Lys^{23} are consistent in showing the least mobility of the four lysine-labeling sites.

When AChBP bound, the anisotropy decay profiles of the FITC toxins were again described by a bi-exponential expression (eq 7) with the ϕ_{slow} values of the FITC-Lys^{35}, -Lys^{49}, and -Lys^{69} conjugates ranging between 17 and 25 ns and a value of 69 ns for the FITC-Lys^{23} conjugate (Figure 6 and Table 3). The ϕ_{slow} values of the FITC-Lys^{35}, -Lys^{49}, and -Lys^{69} conjugates are significantly lower than what is

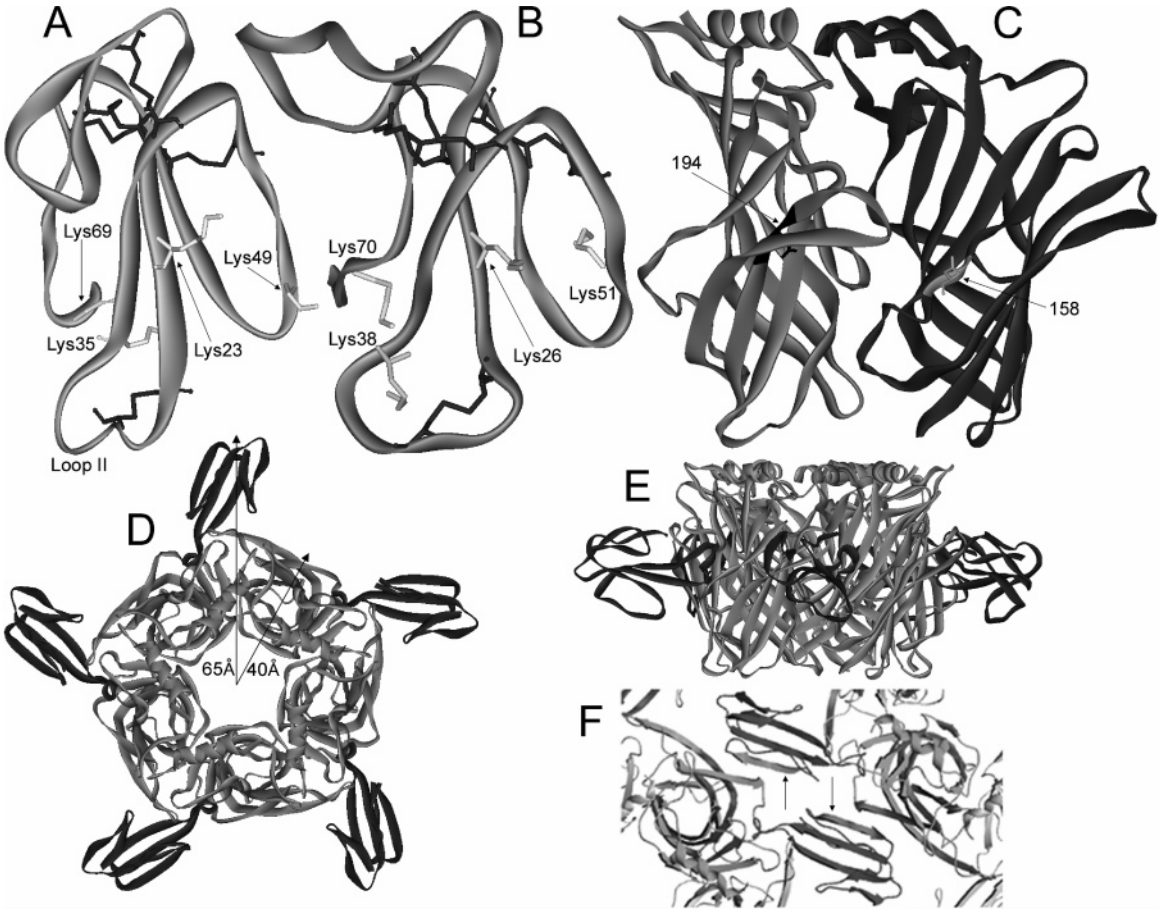

FIGURE 4: Ribbon diagram of the X-ray structures of α-neurotoxins and AChBP. (A) α-Cobratoxin [PDB accession code 2CTX (*40*)]. Average *B* factors for the Lys^{23}, Lys^{35}, Lys^{49}, and Lys^{69} residues from the X-ray coordinates are, respectively, 7.1, 16.3, 27.5, and 54.8, with higher values corresponding to increased disorder. (B) α-Bungarotoxin [PDB accession code 1IDI (*41*)]. (C) Side view of the interface of two AChBP subunits [PDB accession code 1I9B (*5*)]. Cysteine substitutions were made at residues D194C and N158C on opposing sides of the subunit interface and conjugated with the sulfhydryl-reactive probes, MTS-Fl and MTS-EDANS. (D−F) Apical (D), side (E), and crystal lattice packing (F) views of the α-cobratoxin−AChBP complex (PDB accession code 1YI5; figure adapted from ref *7*). Note the interaction between the core structure of the toxin molecule with the core toxin structure in the symmetry-related molecule (arrows in F). The α-carbon backbone and selected side chains are shown in light gray, and disulfide bonds are shown in dark gray.

Table 2: Dissociation Constants for Binding of α-Neurotoxins to AChBP[a]

	K_D (nM)
α-bungarotoxin	1.8[b]
α-cobratoxin	3.2[b]
FITC-Lys^{23}-α-cobratoxin	2.5 ± 0.1
FITC-Lys^{35}-α-cobratoxin	12.6 ± 0.1

[a] Comparison of affinities ± SEM of FITC-labeled α-cobratoxins for AChBP by radioligand-binding competition with [^{125}I]-α-bungarotoxin. [b] Data from ref *15*.

predicted by the Stokes−Einstein equation (81 ns) for a spherical protein with a molecular mass of ~190 kD or the experimental value (142 ns) determined with a longer lifetime reporter group (EDANS) conjugated to the surface of the toxin-bound AChBP (described below). This disparity indicates that the bound-toxin ϕ_{slow} values do not reflect solely whole-body rotational processes but probably a merging of large amplitude α-carbon backbone fluctuations of the AChBP-bound α-neurotoxins with rotational diffusion of the toxin−AChBP complex. The merging of the bound-toxin backbone fluctuations with whole-body diffusional processes makes quantitative assessment of the backbone mobility of the bound α-neurotoxins problematic, but visual inspection of the time course of the anisotropy decay profiles (Figure

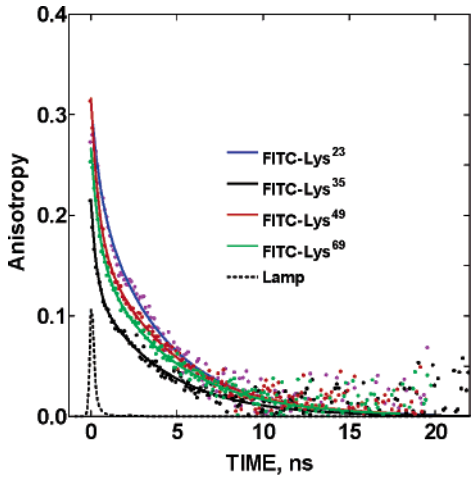

FIGURE 5: Time-resolved fluorescence anisotropy decay for FITC-labeled α-cobratoxins free in solution.

6) suggests that the rank order of mobility of the reporter groups is Lys^{49} > Lys^{69} > Lys^{35} ≫ Lys^{23}. Additionally, the total deconvolved amplitudes of the observable anisotropy decay ($\beta_1 + \beta_2$; Table 3) showed little or no effect from AChBP binding, indicating that the bound reporter group was not immobilized between the toxin and AChBP.

Table 3: Anisotropy Decay Parameters for FITC-Labeled α-Cobratoxins[a]

toxin conjugate	condition	β_1	β_2	ϕ_{fast} (ns)	ϕ_{slow} (ns)	χ^2_r	$\langle\tau\rangle$ (ns)
FITC-Lys^{23}	free	0.04 ± 0.02	0.17 ± 0.02	1.8 ± 0.2	4.2 ± 0.3	1.6 ± 0.2	2.5 ± 0.1
	bound	0.05 ± 0.01	0.18 ± 0.01	2.6 ± 0.8	69 ± 15	1.6 ± 0.3	3.0 ± 0.1
FITC-Lys^{35}	free	0.10 ± 0.02	0.13 ± 0.01	0.1 ± 0.0	3.5 ± 0.2	1.4 ± 0.2	3.7 ± 0.2
	bound	0.12 ± 0.01	0.11 ± 0.02	2.8 ± 0.2	25 ± 5	1.6 ± 0.2	3.6 ± 0.1
FITC-Lys^{49}	free	0.06 ± 0.02	0.16 ± 0.01	0.6 ± 0.1	4.5 ± 0.5	2.0 ± 0.2	3.1 ± 0.1
	bound	0.10 ± 0.01	0.12 ± 0.01	0.8 ± 0.1	17 ± 2	2.1 ± 0.2	2.8 ± 0.1
FITC-Lys^{69}	free	0.06 ± 0.01	0.15 ± 0.01	0.5 ± 0.1	4.3 ± 0.7	1.7 ± 0.2	3.5 ± 0.1
	bound	0.08 ± 0.01	0.14 ± 0.01	1.0 ± 0.1	20 ± 2	2.2 ± 0.6	3.4 ± 0.1

[a] To assess regional variations in toxin flexibility, anisotropy decay of free and AChBP-bound FITC-α-cobratoxins was monitored and fit to a bi-exponential decay equation as described in the Materials and Methods. β_1 and β_2 are the magnitudes of the decay associated with fast and slow processes, respectively. ϕ_{fast} and ϕ_{slow} are the fast and slow rotational correlation times, respectively. χ^2_r is the reduced χ^2 of the anisotropy decay analysis. $\langle\tau\rangle$ is the amplitude-weighted average fluorescence lifetime. In all experiments, α-neurotoxins were present at 0.1 μM, and when applicable, AChBP was present at 0.2 μM in binding site concentration. All data are the average of at least three replicate experiments ± standard deviation.

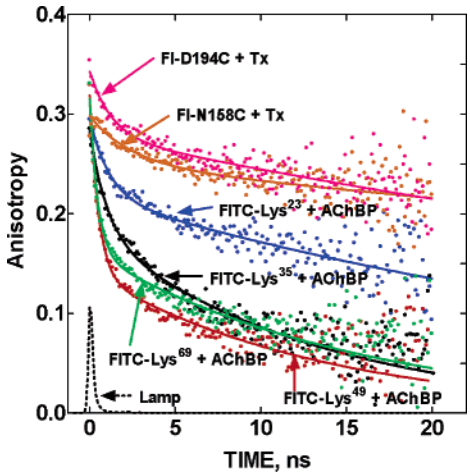

FIGURE 6: Comparison of the time-resolved fluorescence anisotropy decay for AChBP-bound FITC-labeled α-cobratoxins with Fl-N158C-AChBP and Fl-D194C-AChBP complexed with α-bungarotoxin.

To support our interpretation of the fast ϕ_{slow} values for the AChBP-bound FITC-Lys^{35}, -Lys^{49}, and -Lys^{69} conjugates, the anisotropy decay of fluorescein conjugated to two sites on the surface of α-toxin-bound AChBP (Fl-N158C and Fl-D194C) were measured and compared to that of the AChBP-bound FITC-α-neurotoxins. The anisotropy decay of the Fl-AChBP conjugates was measured in the absence and presence of a stoichiometric excess of α-neurotoxin (Table 4 and Figure 7). Similar to the FITC-α-neurotoxins, the anisotropy decay profiles of the Fl-N158C and Fl-D194C mutants were well-fit to an expression for bi-exponential decay (eq 7). The presence of excess α-neurotoxin was associated with significant changes in virtually all of the anisotropy decay parameters (Table 4), indicating that the α-toxin binds to the conjugated AChBP mutants. Focusing on the rotational correlation times of the slow depolarization processes, the ϕ_{slow} values of the Fl-N158C and Fl-D194C conjugates ranged between 86 and 156 ns, which are substantially greater than the comparable values of the AChBP-bound FITC-Lys^{35}, -Lys^{49}, and -Lys^{69} conjugates (range between 17 and 25 ns). The ϕ_{slow} value for the AChBP-bound FITC-Lys^{23} conjugate was intermediate in magnitude (69 ns) between the other FITC and Fl conjugates as described above. Relative to the sites of Fl conjugation on AChBP, three of the four sites of FITC conjugation (Lys^{35}, Lys^{49}, and Lys^{69}) on the AChBP-bound α-neurotoxin were dramatically more flexible than AChBP-surface sites examined and demonstrate the high level of flexibility of much of the AChBP-bound α-neurotoxin.

To obtain a more accurate measure of the averaged whole-body rotational correlation time of α-neurotoxin-bound and free AChBP, the D194C AChBP mutant was conjugated with MTS-EDANS, whose longest emission lifetime is ~20 ns. The anisotropy decay of this conjugate was measured in the presence and absence of excess α-toxin (Table 4 and Figure 7). In the absence of α-neurotoxin, it was possible to fit the anisotropy decay by using the impulse reconvolution method discussed in the Materials and Methods, which yielded a ϕ_{slow} value of 124 ns. When α-neurotoxin was bound, the anisotropy increased slightly during the initial 0.6 ns and then decreased almost mono-exponentially. Consequently, for this sample, the anisotropy decay was fit to eq 7 without impulse reconvolution utilizing the data points starting just after the end of the lamp pulse ($t = 0.8$ ns), which yielded a ϕ_{slow} value of 142 ns, a 15% increase of the value of apo-AChBP.

DISCUSSION

Hydrodynamic Characteristics of an Oligomeric Pore Protein. The unique structure of AChBP as a homomeric pentamer with a C_{5v} axis of symmetry (*30*) protruding through what serves as an open vestibule in the nAChR (*31*) presents some new considerations in the hydrodynamic analysis of oligomeric proteins. Comparable tabulated f/f_0 values for prolate and oblate ellipsoids yield axial ratios between 6 and 10 (*32*), a dimensional asymmetry far greater than one would estimate based simply on dimensions from the crystal structure of the cylindrical pentamer (62 Å in length and 80 Å in diameter). One conclusion is that the expanded hydrodynamic radius due to structured water in the central vestibule contributes significantly to the frictional drag that the AChBP pentamer experiences in translational diffusion. In high resolution X-ray structures of AChBP, one observes symmetrically structured water molecules at the narrow portion of the vestibule that could form a constriction point for ion flow in the full-length receptor (*33*−*35*).

As an initial approximation of molecular dimensions, AChBP might be considered in terms of two concentric cylinders. The inner cylinder would define the volume and surface area of the internal vestibule, whereas the outer cylindrical surface area would define the external solvent exposure. The volume difference between the two cylinders is where the protein mass lies. With an averaged vestibule

Table 4: Anisotropy Decay Parameters for MTS-Fl- and MTS-EDANS-Labeled AChBP[a]

AChBP construct	ligand	β_1	β_2	ϕ_{fast} (ns)	ϕ_{slow} (ns)	χ^2_r	$\langle\tau\rangle$
Fl-N158C	none	0.06 ± 0.01	0.18 ± 0.02	3.0 ± 0.5	90 ± 19	1.7 ± 0.2	3.5 ± 0.1
	α-bungarotoxin	0.03 ± 0.01	0.24 ± 0.01	6.2 ± 0.3	156 ± 14	2.3 ± 0.3	3.8 ± 0.1
Fl-D194C	none	0.05 ± 0.02	0.21 ± 0.02	5.4 ± 1.4	76 ± 16	2.0 ± 0.3	3.0 ± 0.1
	α-bungarotoxin	0.03 ± 0.01	0.26 ± 0.02	3.7 ± 0.2	86 ± 14	1.9 ± 0.7	3.1 ± 0.1
EDANS-D194C	none	0.02 ± 0.01	0.28 ± 0.01	15.0 ± 4.0	124 ± 12	1.0 ± 0.2	17.0 ± 0.1
	α-bungarotoxin[b]	0.01 ± 0.00	0.27 ± 0.01	4.4 ± 0.8	142 ± 14	1.0 ± 0.1	16.8 ± 0.2

[a] To assess regional variations in α-carbon backbone flexibility of AChBP ± α-neurotoxin, anisotropy decays of MTS-Fl-labeled AChBPs were monitored and fit to a bi-exponential decay equation as described in the Materials and Methods. The same approach was taken with MTS-EDANS-labeled AChBP to better estimate the effect of α-toxin binding on the rotational correlation times of AChBP. β_1 and β_2 are the magnitudes of the decay associated with fast and slow processes, respectively. ϕ_{fast} and ϕ_{slow} are the fast and slow rotational correlation times, respectively. χ^2_r is the reduced χ^2 of the anisotropy decay analysis. $\langle\tau\rangle$ is the amplitude-weighted average fluorescence lifetime. All data are the average of at least three replicate experiments ± standard deviation. [b] In the case of α-bungarotoxin bound to EDANS-D194C, anisotropy decay data were analyzed by fitting to eq 7 (see the Materials and Methods) without deconvolution of the lamp pulse starting at a time point 0.8 ns after the peak lamp intensity. Similar experiments were done with α-cobratoxin, and no significant difference between the two α-neurotoxins was observed. Fl-N158C and Fl-D194C were present at 1−2 μM in binding site concentration; EDANS-D194C was present at 3−5 μM; and when applicable, α-bungarotoxin was added to achieve a 1.5-fold stoichiometric excess.

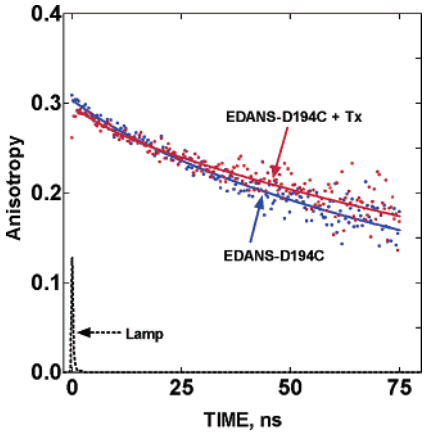

FIGURE 7: Comparison of the time-resolved fluorescence anisotropy decay curves for EDANS-D194C-AChBP alone and complexed with α-bungarotoxin.

radius of 9 Å, the internal volume is 16 000 Å^3 and the internal surface area is 3500 Å^2. The overall volume including the vestibule is 311 000 Å^3, and the corresponding surface area is 15 600 Å^2. Hence, the volume of the outer cylinder is 295 000 Å^3, and its surface area is 12 100 Å^2. Estimated from the central axis of the vestibule to the outer Connolly surface, toxin binding would extend the overall radius of AChBP from 40 to 65 Å, with the maximal length at the tips (Figure 4D).

Structural Fluctuations in AChBP-Bound α-Neurotoxin. Combining hydrodynamic analyses with measurements of fluorescence anisotropy decay enabled us to consider torsional and segmental motion within the molecule in relation to global rotational and translational diffusion parameters revealed by the two experimental approaches.

On the basis of the radial propeller bladelike positioning of five α-neurotoxin molecules around the perimeter of AChBP as shown in the recent X-ray crystal structure (*7*), we anticipated that binding of α-neurotoxin would have a marked influence on the sedimentation properties of AChBP. We assessed the effective distortion of the hydrodynamic shape by sedimentation velocity analysis, which allows one to calculate a frictional coefficient. The ratio, f/f_0, indicates how much the hydrated shape of the experimental protein through its dimensional asymmetry deviates from a compact, nonhydrated sphere. Upon α-neurotoxin binding to AChBP, no significant increase in f/f_0 is observed in contrast to what might be expected if the five toxin molecules were oriented in rigid radial positions as shown in the crystal structure (parts D and E of Figure 4). These data indicate that binding of α-neurotoxin has a minimal effect on the translational diffusion properties of AChBP beyond that predicted from a simple addition of the equivalent compact molecular mass. A parsimonious explanation for this stems from flexibility of the core of the toxin molecule that is likely imparted by joints in the toxin fingers permitting segmental motion of the core disulfide structure. Accordingly, we sought a comparison between motion in the binding protein and the bound-toxin molecule.

Analysis of Segmental Motion by Decay of Fluorescence Anisotropy. Because time-resolved fluorescence anisotropy decay analysis allows one to monitor torsional and segmental motion in proteins as well as their global rotational diffusion, we employed this technique not only to examine global rotation of AChBP and its complex but also, more importantly, to assess the flexibility of bound α-neurotoxin at four positions on the toxin molecule in relation to stationary reference positions on AChBP itself. We found that when the α-neurotoxin is bound to AChBP, the majority of the α-neurotoxin structure remains quite flexible relative to AChBP itself. The exception was at position Lys^{23}, which showed slower segmental motion of limited amplitude upon binding such that its backbone mobility was comparable to that of the F loop of AChBP (F1-N158C).

In light of the α-cobratoxin−AChBP crystal structure (*7*), a high degree of flexibility is not surprising at the loop III position (Lys^{49}) or at the C terminus (Lys^{69}) of the α-neurotoxin, because these regions do not appear to interact directly with the surface of AChBP. However, it is noteworthy that the α-carbon backbone region around Lys^{35} in the α-neurotoxin exhibits greater mobility than that around Lys^{23}. At first inspection, these results are somewhat surprising because Lys^{35} is closer to the tip of loop II and the site of interaction with the binding interface. This residue also appears sandwiched against the C loop of AChBP. If the toxin were behaving as a relatively rigid entity with a fulcrum at the tip of loop II, one might expect movement over a greater segmental arc as one extends from the fulcrum point. However, a closer examination of the crystal structure of the toxin reveals that Lys^{23} is structured in a β-pleated sheet, whereas Lys^{35} is in a loop that lacks secondary structure.

One can consider the motion of the toxin region near Lys^{23} as being restricted by two factors, its surrounding secondary structure and the overall immobilization of the toxin via its interaction at the tip of loop II with AChBP. Therefore, the kinetic component with the dominant amplitude contributing to the decay of anisotropy from FITC-Lys^{23} approaches that of the global rotation rates of the entire complex. The immediate region surrounding Lys^{35} of the toxin, being less constrained by secondary structure, reveals additional segmental motion contributing to the decay of anisotropy from FITC labeled at this site. These data are in agreement with NMR experiments using α-cobratoxin bound to a short C-loop peptide cognate (*36*), wherein an overlay of 10 solution structures of the toxin reveals a single orientation for Lys^{23}, whereas the side chain and α-carbon backbone of Lys^{35} undergo at least a 180° rotation even while bound to the short C-loop peptide mimic.

To impart a frame of reference for assessing segmental motion in α-neurotoxin, we examined time-resolved fluorescence anisotropy decay from two different sites of MTS-Fl conjugation in AChBP itself (D194C and N158C). Data from both sites that lie on opposing sides of the subunit interface indicate far less α-carbon backbone flexibility than we observed from the bound α-neurotoxin. Using MTS-EDANS, a longer lifetime fluorescent probe, labeled at the D194C site in AChBP, enabled us to monitor the slow component of the anisotropy decay that corresponds to the global rotation rate of the macromolecule (Table 4).

To compare our experimentally determined rotational correlation times to a hypothetical value, from the Stokes−Einstein equation, we calculated theoretical rotational correlation times for apo and α-neurotoxin-bound AChBP. Using the molecular weights determined by mass spectrometry, this equation yields rotational correlation times of 64 ns for apo AChBP (from HEK 293 cells) and 81 ns for the α-neurotoxin−AChBP complex. These estimated values, which do not account for associated water, are much lower than the experimentally determined values of 124 and 142 ns, respectively. The structured, retained water in the vestibule of AChBP and associated hydration of the oligosaccharide and other surface residues increase the effective mass and immobilized volume of the molecule. An increase of 26% in rotational correlation times calculated from apo and α-neurotoxin-bound AChBP is slightly greater than the 15% increase in the experimentally determined values. Consistent with the translational hydrodynamic analyses, the small increase in the experimentally determined rotational correlation time indicates that the influence of the bound α-neurotoxin to rotational diffusion can be accounted for simply by the molecular-weight addition and not an increase in dimensional asymmetry in the complex.

A comparison of the time-resolved fluorescence anisotropy decay curves of MTS-Fl and MTS-EDANS conjugated D194C in AChBP reveals differences in probe sensitivity to the segmental and whole-body motions. In preliminary studies, MTS-Fl conjugates of AChBP were consistently more sensitive to ligand-induced changes in fast segmental motions, while MTS-EDANS more reliably reported on the whole-body rotational diffusion (Hibbs, R. E. and Johnson, D. A., unpublished observations). The capacity of MTS-EDANS conjugates to measure this slow rotational decay component arises primarily from longer emission lifetimes ($\langle\tau\rangle \sim 17$ ns) than MTS-fluorescein conjugates ($\langle\tau\rangle \sim 3$ ns). The diminished capacity of MTS-EDANS conjugates to monitor segmental motions may be due to their longer tether arm (eight versus five atoms) and/or the amphipathic character of the reporter group.

Elapid α-neurotoxins exhibit a high degree of subtype selectivity for nAChRs. Their highest affinity is found for the muscle receptors from vertebrate species, yet certain residue substitutions and glycosylation can make certain animal species more resistant to the three-fingered α-neurotoxins than others (*37*−*39*). Many neuronal receptors are resistant to the α-neurotoxins, yet the homomeric neuronal species, typified by α7, show high affinities for the long neurotoxins. AChBP thus will serve as a structural template for the nicotinic receptor subtypes, and through mutagenesis, it should be possible to replicate the affinity changes and presumably ascertain the α-neurotoxin-binding determinants of the various receptor subtypes. A suggestion that the nAChR and AChBP determinants are not identical comes from a comparison of the anisotropy decay data where the fluorescein conjugated at residue 69 in the nAChR-bound toxin shows a faster initial rate of decay than the other substituted lysines (*29*). In the case of AChBP, the fluorescein decay rate at position 69 is not distinguishable from that at residues 35 and 49 (Table 3 and Figure 6).

In summary, hydrodynamic measurements of translational diffusion and time-resolved fluorescence anisotropy decay analyses of rotational diffusion and intrinsic segmental motion yield a consistent picture of the dynamics of the AChBP-bound α-neurotoxin molecules. Internal motion of the α-neurotoxin molecule imparted by flexibility in the peptide chains in the α-neurotoxin fingers allows for the core of the molecule to move segmentally in a limited conical arc independent of the pentameric complex. This is demonstrated in lower resistance to rotational and translational diffusion than would be predicted from rigid α-neurotoxin molecules extended radially from the AChBP surface. Furthermore, time-resolved fluorescence anisotropy decay reveals additional degrees of segmental motion of the α-neurotoxin core not evident in the residues found on the binding interface of AChBP.

REFERENCES

1. Karlin, A. (2002) Emerging structure of the nicotinic acetylcholine receptors, *Nat. Rev. Neurosci. 3*, 102−114.
2. Nirthanan, S., and Gwee, M. C. (2004) Three-finger α-neurotoxins and the nicotinic acetylcholine receptor, 40 years on, *J. Pharmacol. Sci. 94*, 1−17.
3. Changeux, J. P., Kasai, M., and Lee, C. Y. (1970) Use of a snake venom toxin to characterize the cholinergic receptor protein, *Proc. Natl. Acad. Sci. U.S.A. 67*, 1241−1247.
4. Taylor, P., Molles, B., Malany, S., and Osaka, H. (2002) in *Perspectives in Molecular Toxinology* (Menez, A., Ed.) pp 271−280, John Wiley and Sons, Chichester, U.K.
5. Brejc, K., van Dijk, W. J., Klaassen, R. V., Schuurmans, M., van Der Oost, J., Smit, A. B., and Sixma, T. K. (2001) Crystal structure of an ACh-binding protein reveals the ligand-binding domain of nicotinic receptors, *Nature 411*, 269−276.
6. Bouzat, C., Gumilar, F., Spitzmaul, G., Wang, H. L., Rayes, D., Hansen, S. B., Taylor, P., and Sine, S. M. (2004) Coupling of agonist binding to channel gating in an ACh-binding protein linked to an ion channel, *Nature 430*, 896−900.
7. Bourne, Y., Talley, T. T., Hansen, S. B., Taylor, P., and Marchot, P. (2005) Crystal structure of a Cbtx−AChBP complex reveals essential interactions between snake α-neurotoxins and nicotinic receptors, *EMBO J. 24*, 1512−1522.

8. Harel, M., Kasher, R., Nicolas, A., Guss, J. M., Balass, M., Fridkin, M., Smit, A. B., Brejc, K., Sixma, T. K., Katchalski-Katzir, E., Sussman, J. L., and Fuchs, S. (2001) The binding site of acetylcholine receptor as visualized in the X-ray structure of a complex between α-bungarotoxin and a mimotope peptide, *Neuron 32*, 265−275.
9. Antil-Delbeke, S., Gaillard, C., Tamiya, T., Corringer, P. J., Changeux, J. P., Servent, D., and Menez, A. (2000) Molecular determinants by which a long chain toxin from snake venom interacts with the neuronal α 7-nicotinic acetylcholine receptor, *J. Biol. Chem. 275*, 29594−29601.
10. Fruchart-Gaillard, C., Gilquin, B., Antil-Delbeke, S., Le Novere, N., Tamiya, T., Corringer, P. J., Changeux, J. P., Menez, A., and Servent, D. (2002) Experimentally based model of a complex between a snake toxin and the α 7 nicotinic receptor, *Proc. Natl. Acad. Sci. U.S.A. 99*, 3216−3221.
11. Malany, S., Osaka, H., Sine, S. M., and Taylor, P. (2000) Orientation of α-neurotoxin at the subunit interfaces of the nicotinic acetylcholine receptor, *Biochemistry 39*, 15388−15398.
12. Osaka, H., Malany, S., Molles, B. E., Sine, S. M., and Taylor, P. (2000) Pairwise electrostatic interactions between α-neurotoxins and γ, δ, and ϵ subunits of the nicotinic acetylcholine receptor, *J. Biol. Chem. 275*, 5478−5484.
13. Reynolds, J. A., and Karlin, A. (1978) Molecular weight in detergent solution of acetylcholine receptor from *Torpedo californica*, *Biochemistry 17*, 2035−2038.
14. Karlsson, E., Arnberg, H., and Eaker, D. (1971) Isolation of the principal neurotoxins of two *Naja naja* subspecies, *Eur. J. Biochem. 21*, 1−16.
15. Hansen, S. B., Radic, Z., Talley, T. T., Molles, B. E., Deerinck, T., Tsigelny, I., and Taylor, P. (2002) Tryptophan fluorescence reveals conformational changes in the acetylcholine binding protein, *J. Biol. Chem. 277*, 41299−41302.
16. Hibbs, R. E., Talley, T. T., and Taylor, P. (2004) Acrylodan-conjugated cysteine side chains reveal conformational state and ligand site locations of the acetylcholine-binding protein, *J. Biol. Chem. 279*, 28483−28491.
17. Reeves, P. J., Callewaert, N., Contreras, R., and Khorana, H. G. (2002) Structure and function in rhodopsin: High-level expression of rhodopsin with restricted and homogeneous N-glycosylation by a tetracycline-inducible *N*-acetylglucosaminyltransferase I-negative HEK293S stable mammalian cell line, *Proc. Natl. Acad. Sci. U.S.A. 99*, 13419−13424.
18. Hansen, S. B., Sulzenbacher, G., Huxford, T., Marchot, P., Taylor, P., and Bourne, Y. (2005) Structures of *Aplysia* AChBP complexes with nicotinic agonists and antagonists reveal distinctive binding interfaces and conformations, *EMBO J. 24*, 3635−3646.
19. Johnson, D. A., and Cushman, R. (1988) Purification and characterization of four monofluorescein cobra α-toxin derivatives, *J. Biol. Chem. 263*, 2802−2807.
20. Correia, J. J. (2000) Analysis of weight average sedimentation velocity data, *Methods Enzymol. 321*, 81−100.
21. Laue, T. M., Shah, B. D., Ridgeway, T. M., and Pelletier, S. L. (1992) *Analytical Ultracentrifugation in Biochemistry and Polymer Science*, Royal Society of Chemistry, Cambridge, U.K.
22. Cantor, C. R., and Schimmel, P. R. (1980) in *Biophysical Chemistry* (Bartlett, A. C., Vapnek, P. C., and McCombs, L. W., Eds.) pp 539−641, W. H. Freeman and Company, San Francisco, CA.
23. Birch, D. J. S., and Imhof, R. E. (1991) in *Topics in Fluorescence Spectroscopy: Techniques* (Lakowicz, J. R., Ed.) Plenum, New York.
24. Gangal, M., Cox, S., Lew, J., Clifford, T., Garrod, S. M., Aschbaher, M., Taylor, S. S., and Johnson, D. A. (1998) Backbone flexibility of five sites on the catalytic subunit of cAMP-dependent protein kinase in the open and closed conformations, *Biochemistry 37*, 13728−13735.
25. Li, F., Gangal, M., Jones, J. M., Deich, J., Lovett, K. E., Taylor, S. S., and Johnson, D. A. (2000) Consequences of cAMP and catalytic-subunit binding on the flexibility of the A-kinase regulatory subunit, *Biochemistry 39*, 15626−15632.
26. Boyd, A. E., Dunlop, C. S., Wong, L., Radic, Z., Taylor, P., and Johnson, D. A. (2004) Nanosecond dynamics of acetylcholinesterase near the active center gorge, *J. Biol. Chem. 279*, 26612−26618.
27. Shi, J., Tai, K., McCammon, J. A., Taylor, P., and Johnson, D. A. (2003) Nanosecond dynamics of the mouse acetylcholinesterase Cys69−Cys96 ω loop, *J. Biol. Chem. 278*, 30905−30911.
28. Cantor, C. R., and Schimmel, P. R. (1980) in *Biophysical Chemistry* (Bartlett, A. C., Vapnek, P. C., and McCombs, L. W., Eds.) pp 459−461, W. H. Freeman and Company, San Francisco, CA.
29. Johnson, D. A. (2005) C-Terminus of a long α-neurotoxin is highly mobile when bound to the nicotinic acetylcholine receptor: A time-resolved fluorescence anisotropy approach, *Biophys. Chem. 116*, 213-218.
30. Wilson, E. B., Decius, J. C., and Cross, P. C. (1955) in *Molecular Vibrations: The Theory of Infrared and Raman Vibrational Spectra*, pp 77−101, McGraw-Hill Book Company, Inc., New York.
31. Unwin, N. (1993) Nicotinic acetylcholine receptor at 9 Å resolution, *J. Mol. Biol. 229*, 1101−1124.
32. Cantor, C. R., and Schimmel, P. R. (1980) in *Biophysical Chemistry* (Bartlett, A. C., Vapnek, P. C., and McCombs, L. W., Eds.) pp 561, W. H. Freeman and Company, San Francisco, CA.
33. Celie, P. H., Klaassen, R. V., van Rossum-Fikkert, S. E., van Elk, R., van Nierop, P., Smit, A. B., and Sixma, T. K. (2005) Crystal structure of acetylcholine-binding protein from *Bulinus truncatus* reveals the conserved structural scaffold and sites of variation in nicotinic acetylcholine receptors, *J. Biol. Chem. 280*, 26457−26466.
34. Hansen, S. B., Sulzenbacher, G., Huxford, T., Marchot, P., Taylor, P., and Bourne, Y. (2005) Structures of *Aplysia* AChBP complexes with agonists and antagonists reveal distinctive binding interfaces and conformations, manuscript submitted for publication.
35. Hibbs, R. E., Hansen, S. B., Talley, T. T., Kem, W. R., and Taylor, P. (2005) Unpublished results (1.7 Å).
36. Zeng, H., and Hawrot, E. (2002) NMR-based binding screen and structural analysis of the complex formed between α-cobratoxin and an 18-mer cognate peptide derived from the α 1 subunit of the nicotinic acetylcholine receptor from *Torpedo californica*, *J. Biol. Chem. 277*, 37439−37445.
37. Kachalsky, S. G., Jensen, B. S., Barchan, D., and Fuchs, S. (1995) Two subsites in the binding domain of the acetylcholine receptor: An aromatic subsite and a proline subsite, *Proc. Natl. Acad. Sci. U.S.A. 92*, 10801−10805.
38. Barchan, D., Kachalsky, S., Neumann, D., Vogel, Z., Ovadia, M., Kochva, E., and Fuchs, S. (1992) How the mongoose can fight the snake: The binding site of the mongoose acetylcholine receptor, *Proc. Natl. Acad. Sci. U.S.A. 89*, 7717−7721.
39. Barchan, D., Ovadia, M., Kochva, E., and Fuchs, S. (1995) The binding site of the nicotinic acetylcholine receptor in animal species resistant to α-bungarotoxin, *Biochemistry 34*, 9172−9176.
40. Betzel, C., Lange, G., Pal, G. P., Wilson, K. S., Maelicke, A., and Saenger, W. (1991) The refined crystal structure of α-cobratoxin from *Naja naja siamensis* at 2.4 Å resolution, *J. Biol. Chem. 266*, 21530−21536.
41. Zeng, H., Moise, L., Grant, M. A., and Hawrot, E. (2001) The solution structure of the complex formed between α-bungarotoxin and an 18-mer cognate peptide derived from the α 1 subunit of the nicotinic acetylcholine receptor from *Torpedo californica*, *J. Biol. Chem. 276*, 22930−22940.

BI051735P